PAPER

Check for updates

Fluorine mapping *via* LA-ICP-MS/MS: a proof of concept for biological and geological specimens

David Clases,†*[a] Raquel Gonzalez de Vega, [iD] †[a] John Parnell[b] and Jörg Feldmann[a]

Fluorine (F) plays an important role in biology and geology but is hard to analyse and quantify using element-specific techniques. This is related to its high first ionisation potential and analytical methods depending on high energy sources for excitation and/or ionisation of F. In particular ICP-MS was initially found incapable of detecting F; however, recent methodological advances, *i.e.*, the application of Ba as a plasma modifier and the application of tandem mass spectrometry, enabled its analysis by targeting BaF^+. In this study, we suggest this approach in conjunction with laser ablation to perform the mapping of F in both biological and geological samples. In a proof of concept, tooth samples as biological samples and a Rhynie chert as a geological sample were analysed. For method development and to evaluate the performance of the developed method, gelatine-based F-standards were prepared and characterised using combustion ion chromatography. Standards were further interrogated to estimate LODs and LOQs. Depending on the required spatial resolution, figures of merit in the upper ng g^{-1} range and lower µg g^{-1} range were achievable. This is the first example of F mapping using LA-ICP-MS instrumentation and the developed methods close an important analytical gap by enabling the spatially resolved F analysis at relevant biological and geological concentrations.

Introduction

Fluorine (F) is a ubiquitous element impacting biology and geology. As an element with the highest electronegativity, it occurs naturally almost exclusively as fluoride ($F^−$).[1] However, due to industrial use as well as application in pharmaceuticals, increasing amounts of fluorinated organic molecules can be found in the global environment. While $F^−$ can be relevant for dental health,[2,3] a plethora of organic F-species, such as poly- and perfluoroalkyl substances (PFASs),[4] are causing increasing concerns and some have been categorised as carcinogens.[5] Due to the natural role of $F^−$ in the lithosphere and its increasing discharge due to anthropogenic sources, qualitative and quantitative analytical methods are in high demand and should ideally be capable of detecting F in both the aqueous and terrestrial environments and distinguishing between different chemical species. A relatively recent technique for the analysis of F is inductively coupled plasma-mass spectrometry (ICP-MS).[6] Due to its high first ionisation potential and the limited ion yield in the plasma, F analysis *via* ICP-MS was originally considered impracticable. However, in 2017 Jamari *et al.* suggested the exploitation of polyatomic F-

ions, which can be formed in the plasma through the addition of different modifiers.[6] Ba^{2+} solutions with levels around 100 µg mL^{-1} turned out to be efficient for the formation of BaF^+, which could subsequently be targeted as a proxy for F levels across a concentration range spanning from the mid ng mL^{-1} to the upper µg mL^{-1} range. This approach was adopted for elemental speciation analysis of F using LC-ICP-MS[7] as well as for the analysis of F-containing particles *via* single particle ICP-MS.[8]

So far, this methodology has not been adopted for LA-ICP-MS, which is the current state of the art for elemental mapping.[9] Enabling F-mapping *via* this technique, however, would close an important analytical gap and promote investigations of relevant biological as well as geological specimens while studying colocalization with relevant trace elements. This is underpinned by the fact that not only the speciation and levels of F stipulate the ecological and biochemical impact, but also its location in highly compartmentalised systems. So far, imaging techniques such as SEM-EDX, AES, LIBS or ToF-SIMS[3,10] have been capable to target F by exploiting highly energetic sources for the excitation and/or ionisation of F. Unfortunately, these methods are impracticable to analyse larger specimens, lack selectivity or sensitivity or require cumbersome sample pre-treatments and conditions of analysis.

This proof of concept demonstrates the first LA-ICP-MS method harnessing the plasma formation of BaF^+ for F-mapping in both biological and geological samples.

[a]Institute of Chemistry, University of Graz, Graz, Austria. E-mail: David.Clases@uni-graz.at

[b]School of Geosciences, University of Aberdeen, Aberdeen, UK

† These authors contributed equally.

Materials and methods

Instrumentation, chemicals, and consumables

An 8900 series ICP-MS/MS system (Agilent Technologies, Santa Clara, CA, USA) was equipped with platinum cones and s-lenses and operated with MassHunter software (Agilent Technologies). A Scott-type double-pass spray chamber was cooled to 2 °C and a MicroMist™ concentric nebuliser (Elemental Scientific Inc., Omaha, NE, US) was used for sample nebulisation. The inner diameter of the torch's injector was 1.4 mm.

Isotopes were analysed with dwell times between 20 and 110 ms. The collision/reaction cell (CRC) was pressured with H_2 (5 mL min^{-1}), He (3.5 mL min^{-1}) and O_2 (15%). He (99.999%) was used a carrier gas to transport the ablated aerosol into the plasma.

Element standards at 1000 µg mL^{-1} (Single-Element ICP-Standard-Solution Roti®Star) were diluted to working concentrations using ultra-pure water (18.2 MΩ cm, Merck Millipore, Bedford, USA). 1 ng mL^{-1} Li, Y, Tl, Ce and Ba were analysed daily to monitor the instrument's performance in a conventional "liquid nebulisation set-up" and a multi-elemental standard was used to set the P/A factor.

For elemental mapping, the ICP-MS/MS system was coupled with an Analyte G2 193 nm excimer laser from Teledyne Photon Machines (Omaha, US), which was set up with an aerosol rapid introduction system (ARIS). HDIP (Teledyne Photon Machines, v.1.7.12.52) was used to optimise the LA-ICP-MS/MS parameters and a fluence of 2.45 J cm^{-2} was employed for ablation. The performance of the LA-ICP-MS/MS method was monitored analysing the "612 NIST – trace metals in glass" SRM. Gelatine for standard preparation was obtained from MM Ingredients (Wimborne, Dorset, UK) and background levels of cations were reduced in an extraction step employing an ion exchange resin (Amberlyst® 15 hydrogen form, Sigma Aldrich) before preparing a blank and spiking 5 levels of F concentrations. The gelatine was mixed for homogenisation and filled into HybriWells obtained from Sigma Aldrich.

Samples, standards and data processing

Tooth samples as well as a chert sample were chosen as representative biological and geological samples, respectively. A deciduous tooth of an 8 year-old child (m) was collected after falling out naturally and a wisdom tooth containing an amalgam filling was obtained from a 57 year-old man following a routine surgical wisdom-teeth removal procedure. The teeth were embedded in epoxy resin, cut, and polished prior to LA analysis.

The chert sample was obtained from Rhynie in northern Scotland. It originates from the Lower Devonian continental succession and consists of sandstones and shales.[11] The sample contained fossilised plant materials. Due to a hot spring activity, silica as well as light elements entered plant cells. The sample was polished and directly analysed.

Although the 612 NIST SRM contained F, it also exhibited significant levels of Gd. Gd has an isotope with 157 amu

Table 1 Fluorine concentrations in the blank and 5 gelatine standards determined *via* CIC. Error is expressed as 1 SD ($n = 3$)

Level	Concentration (µg g^{-1})
Blank	0.00 ± 0.0
1	41.2 ± 5.1
2	69.1 ± 2.4
3	106 ± 4.7
4	190 ± 7.0
5	977 ± 16

(relative abundance: 0.157) interfering with the analysis when monitoring BaF$^+$ at m/z 157. As this complicates method development, purified gelatine standards containing defined amounts of F were manufactured and analysed to find optimal instrumental parameters. Six gelatine standards were prepared by spiking certified F standards into liquified gelatine, which was subsequently mixed and injected in moulds according to a protocol by Westerhausen *et al.*[12]

The exact concentrations of F in the standards were determined by combustion ion chromatography (CIC) after acid digestion and are listed in Table 1. The CIC method was adapted from a study by Schultes *et al.*[13] Briefly, 100 µL of standard digests were injected into a ceramic sample boat containing glass wool and combusted slowly in a combustion furnace (HF-210, Mitsubishi) at 1100 °C under a flow of oxygen (400 L min^{-1}) and argon (200 L min^{-1}) for approximately 7 minutes. Combustion gases were absorbed in Milli-Q water during the entire length of the combustion process using a gas absorber unit (GA-210, Mitsubishi). 100 µL of the absorption solution was injected onto an ion chromatograph (Dionex Aquion RFIC, Thermo Fisher Scientific) equipped with an anion exchange column (Dionex IonPac AS19 2 × 50 mm guard column and AS20 2 × 250 mm analytical column) operated at 35 °C. Chromatographic separation was achieved by running a 25 min gradient of aqueous hydroxide mobile phase ramping from 8 mM to 60 mM at a flow rate of 0.25 mL min^{-1}. F$^-$ was detected using a conductivity detector. Quantification was carried out using a linear six-point calibration curve of NaF ranging from 0.5 to 50 µg mL^{-1} (R^2 = 0.9986). Quality controls consisting of a known concentration of PFOS standard were measured periodically and recovery was 94.9%.

Elemental maps were generated using HDIP (Teledyne Photon Machines, v.1.7.12.52) and Pew^2 software.[14] Figures were created using OriginLab 8.5. Limits of analysis were determined following the ablation of F-gelatine standards and construction of calibration curves. The LOD and LOQ were calculated by dividing three and ten-times the standard deviation at the intercept by the calibration curve's slope, respectively.

The highest F$^-$ standard was further analysed to optimise instrumental parameters for the acquisition of BaF$^+$. Optimised values are listed in Table 2.

1662 | *J. Anal. At. Spectrom.*, 2023, **38**, 1661–1667

This journal is © The Royal Society of Chemistry 2023

Table 2 Experimental parameters of the LA-ICP-MS/MS system

Plasma parameter	Tuning value
Forward power	1600 W
Sampling depth	3.3 mm
Nebuliser flow rate	0.61 L min^{-1}
Make-up flow rate	0.26 L min^{-1}
Cell He-flow rate	0.5 L min^{-1}
Cup He-flow rate	0.4 L min^{-1}
Peristaltic pump	0.04 rpm

Ion optics and CRC	Tune value
Extraction 1	−160.6 V
Extraction 2	−0.5 V
Deflect	2.8 V
AMU offset (Q1)	60
AMU gain (Q1)	146
Energy discrimination	−20.0 V
Octupole bias	−4.8 V
O$_2$ cell flow rate	15%
H$_2$ cell flow rate	3.5 mL min^{-1}
He cell flow rate	5.0 mL min^{-1}
Axial acceleration	1.3 V

Results and discussion

Method development

Due to the high first ionisation potential of F (17.42 eV), the F$^+$ ion yield in the plasma is insignificant. To make F analysis via ICP-MS feasible, a Ba^{2+} solution can be added to the plasma as a modifier to form BaF$^+$, which can be targeted instead of F$^+$. To follow this strategy in LA-ICP-MS, a 100 μg mL^{-1} Ba solution was nebulised and mixed with the dry aerosol originating from the LA-system before entering the injector. The experimental set-up is illustrated in Fig. 1.

The ionisation degree of elements depends on their ionisation energy and various plasma parameters. Typically, tuning procedures aim to find normal analytical zones, which are regions within the plasma with the highest density of targeted elemental cations. Due to varying physical properties of different elements, these regions are located at different plasma depths (z-positions). Therefore, tuning procedures often adapt nebuliser/make-up flow gases, plasma power and/or plasma-z position to align these normal analytical zones with the MS interface for ion extraction. For the sampling of BaF$^+$, this strategy is more complicated as a chemical reaction is required to take place before extraction. The formation of BaF$^+$ in the plasma is possible by the reaction of Ba$^+$ with elemental F as well as the reaction of Ba^{2+} with F$^-$, of which the latter was suggested to be the most important one.[15] Given that the positions of highest densities in the plasma are differently distributed for these entities and that the highest BaF$^+$ levels are expected to form at their interface, tuning for sensitivity is often more difficult as high ion densities are confined to smaller regions. It is worth mentioning that not only the ion density of BaF$^+$ needs to be considered, but also the abundance of interferences which increase background and noise. Therefore, to find optimal figures of merit, signal to noise ratios need to be considered rather than sensitivities alone. While this is cumbersome in solution-based ICP-MS requiring periodical analysis of blanks and standards, LA-ICP-MS offers facilitated evaluation of signal and noise. In this proof of concept study, a gelatine standard containing 977 μg F g^{-1} was prepared and analysed using LA-ICP-MS/MS with a Ba^{2+} modifier (compare Fig. 1) at 2 Hz using a spot size of 150 μm. This procedure allowed rapid periodic analysis of signal and noise as shown in Fig. 2.

The best figures of merit for BaF$^+$ analysed were found at m/z 157 under relatively energetic conditions, which were promoted by the introduction of He[16] (0.9 L min^{-1}) and by limiting the introduction of a wet aerosol into the plasma (peristaltic pump: 0.04 rpm). Optimal BaF$^+$ sampling positions were found in hotter
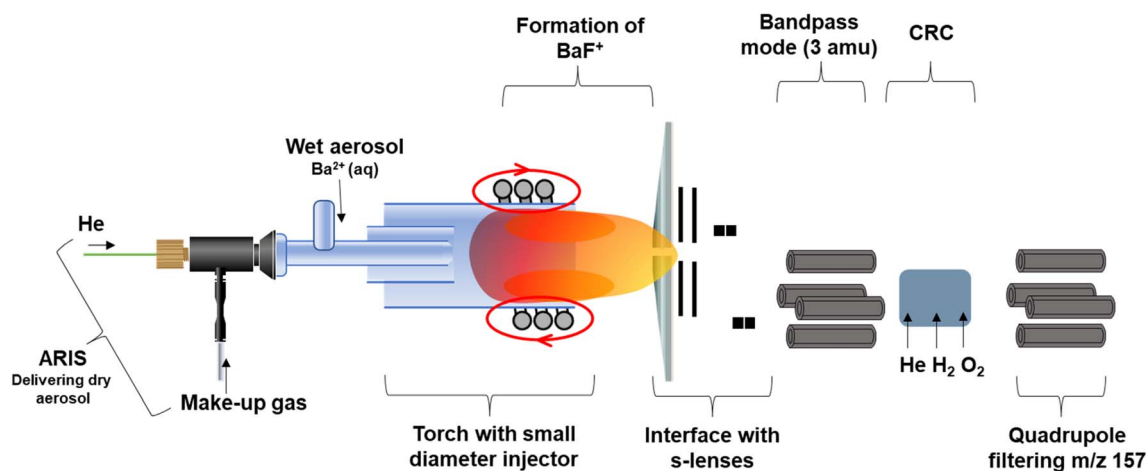

Fig. 1 Instrumental set-up for the mapping of F. The dry aerosol received by the LA system was mixed with a wet aerosol containing Ba^{2+} before the torch. The F from the sample was transported via the dry aerosol generated BaF$^+$ in the plasma, which was extracted and analysed at m/z 157 using an ICP-MS/MS system.
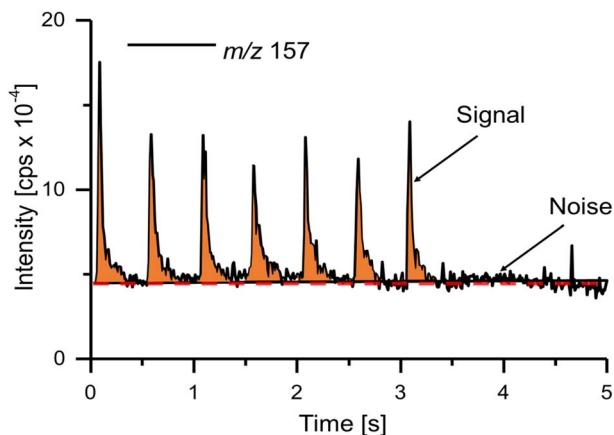
Fig. 2 The analysis of F^- spiked gelatine standards enabled signal and noise events to be resolved facilitating method optimisation. The standard contained 977 µg F g^{-1} and was ablated using a laser beam spot size of 150 µm and 2 Hz laser shot frequency and analysed at m/z 157 (BaF$^+$).

plasma zones closer to the coil (3.3 mm). All relevant plasma parameters are listed in Table 2. S-Lenses were used to employ hard extraction conditions by inverting the polarity of the first and second extraction lenses. This strategy is often used to increase ion transmission as reported for single particle ICP-MS,[17] LA-ICP-MS,[18] and LC-ICP-MS[19] as well as in GC-ICP-MS.[20] However, higher background signals are often concurrent with hard extraction conditions and the overall signal to noise ratios need to be balanced to benefit from higher transmissions. Therefore, method development was performed as demonstrated in Fig. 2 by balancing background, noise and signal. One effective way to limit interferences was the use of a CRC, which allowed BaF$^+$ to be resolved at m/z 157 via chemical and/or physical processes. To limit the ions entering the CRC and to reduce potential interferences further, a MS/MS-set-up for ICP-MS was beneficial as discussed elsewhere.[6,7] Comparing figures of merit using single quadrupole (SQ) and MS/MS conditions, we could confirm significantly reduced background levels of interferences and therefore improved signal to noise ratios when using the latter. However, the best figures of merit were found by finding a compromise between SQ and MS/MS conditions by alteration of the mass bandpass of the first quadrupole. Known as bandpass mode developed for various ICP-MS set-ups including speciation, imaging or single particle analysis,[17–19,21,22] this method enhanced ion transmission by adapting the quadrupole's scanning line via manipulation of its slope and intercept. Using a mass bandwidth of 3 amu, it was possible to increase BaF$^+$ intensities without increasing background significantly. Different cell gas flows and combination of cell gases were optimised empirically. All MS parameters are listed in Table 2.

In this proof of concept, method development and the optimisation of tuning parameters were performed by balancing the signal and noise as shown in Fig. 2. The aim was to develop a method and demonstrate its capability to determine F at relevant levels and resolutions in biological and geological samples. However, it is likely that this method may

be further improved via a more systematic approach to understand the interdependency of various parameters. This in fact may be critical to enhance the understanding of plasma processes and to provide insights into underlying mechanisms which are important for the formation of BaF$^+$.

Figures of merit

Employing the optimised method, a calibration curve was created following the ablation of F$^-$ spiked gelatine standards. This approach was pursued to provide a rough estimation of underlying limits of analysis. It is worth mentioning that the ablation of gelatine and hard biogenic and geogenic specimens is very different. However, it was previously shown that gelatine can be used to prepare homogeneous and smooth standards for LA-ICP-MS when cast in moulds.[12] Given that suitable homogeneous and solid F-based standards for LA-ICP-MS are inaccessible, mould-cast F-spiked gelatine standards offer a useful platform for method development and estimations of figures of merit. As such, rather than providing means for the absolute quantification of F distributions, it was our purpose to deliver a point of reference and to interrogate the method's capabilities. The F$^-$ concentrations in the gelatine standards ranged between 41 and 977 µg g^{-1} as shown in Fig. 3. Data points were fitted (instrumental weighing) and Pearson's R^2 was determined as a measure of linearity (0.9999). The LOD and LOQ were determined to be 2.7 µg g^{-1} and 9.0 µg g^{-1}, respectively, using a laser beam size of 65 µm and a laser shot dosage of 4. The limits of analysis may be improved when adapting laser parameters i.e., sacrificing spatial resolution by increasing dosage and/or laser spot size. For example, using a spot size of 150 µm while conserving all other parameters led to an increased aerosol mass flow resulting in a LOD on the upper ng g^{-1} scale. BaF$^+$ is formed at the interface of the normal analytical zones of Ba^{2+} and F$^-$ and the higher ion yields are confined to a relatively narrow overlap region entailing a destabilising effect on signal intensity as shown by Jamari et al.,[6] and recognisable as increased standard deviations in Fig. 3.

Imaging of fluorine in biomaterials

The most significant natural sources of F exposure are drinking water and food.[23–26] Due to its high affinity to calcium phosphate phases, it is readily integrated into teeth and bones following exposure. To increase the dental health of the population, F$^-$ is often supplemented in public programs.[2,27,28] Following exposure, F$^-$ exchanges with hydroxide in hydroxyapatite to form fluorapatite as part of enamel, which is harder and less prone to caries. Between 200 and 3000 µg g^{-1} was the expected range of F in enamel.

As a proof of concept and to demonstrate the possibility of mapping F next to trace elements such as Cu and Zn, a deciduous tooth and wisdom tooth were analysed. Fig. 4 shows the elemental analysis of the latter. Cu and Zn were targeted as essential elements and Hg was analysed as a proxy for an amalgam filling. To avoid a false positive detection of BaF$^+$ due to ^{157}Gd$^+$ as isobaric interference, Gd was additionally monitored at m/z 160 but exhibited only negligible levels. F was located on the outside areas of the teeth, which is consistent
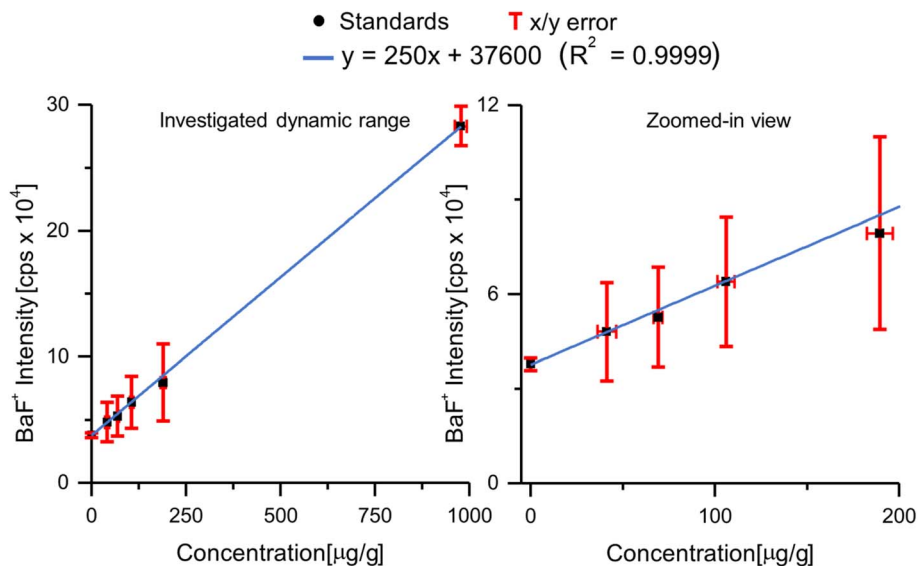
Fig. 3 The calibration curve obtained from the analysis of gelatine standards was used for the estimation of figures of merit. The *x* error expresses 1 SD of the concentration (*n* = 3) and the *y* error expresses the standard deviation across recorded data points (*n* = 30).
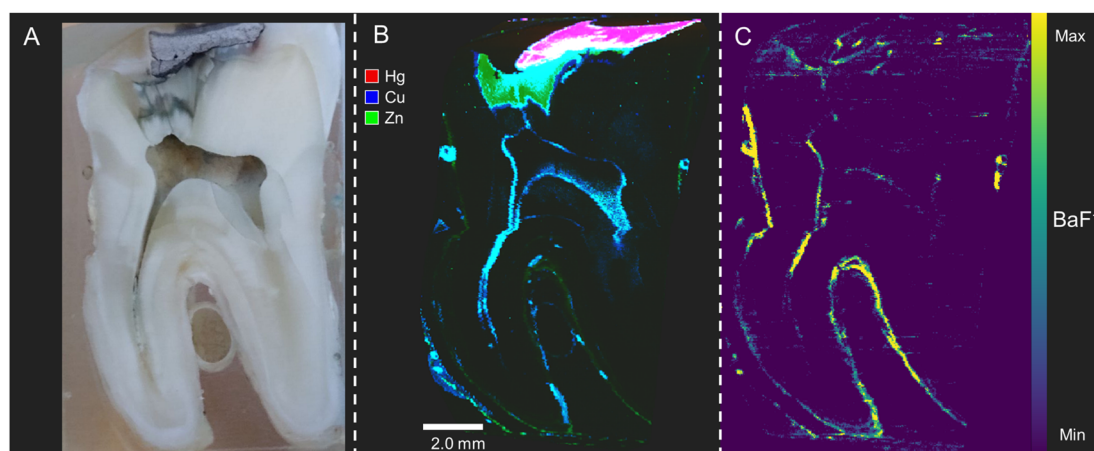

Fig. 4 (A) Photograph of the analysed wisdom tooth containing an amalgam filling. (B) Hg, Cu and Zn were analysed as elements contained in the filling and in endogenous tooth structures such as root channels. (C) Distribution of F in the tooth. An accumulation in the interior close to channels as well as on the outside of the tooth is visible.

with F^- having direct contact with surface enamel and undergoing the exchange reaction to fluorapatite.

Fig. 5 shows the analysis of F in a deciduous tooth. The highest F levels were detected on outside areas; however, also

Fig. 5 F distribution in a deciduous tooth.

within the tooth a F line was distinguishable. This is in accordance with a study by Martinez *et al.*,[3] who employed LIBS to image the F distribution in the teeth of children. They found different pre- and postnatal F levels and found higher levels close to the neonatal line.
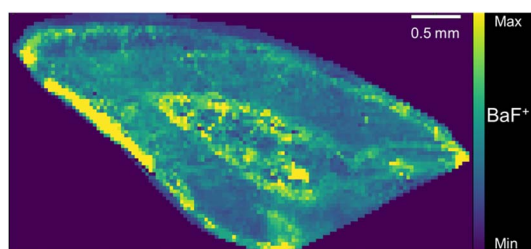
Imaging of F in geological samples

As the thirteenth most abundant element in the Earth's crust, F exists mostly in minerals such as fluorite, fluorapatite and cryolite. Its average mass-based levels in the continental crust amount to about 550 $\mu g\ g^{-1}$ and it plays an important role in geochemical and biogeochemical systems.[29] The abundance and spatial distribution of F are highly variable and are for example influenced by hydrothermal alterations, mineralisation and weathering.[29] However, our knowledge of the role of F
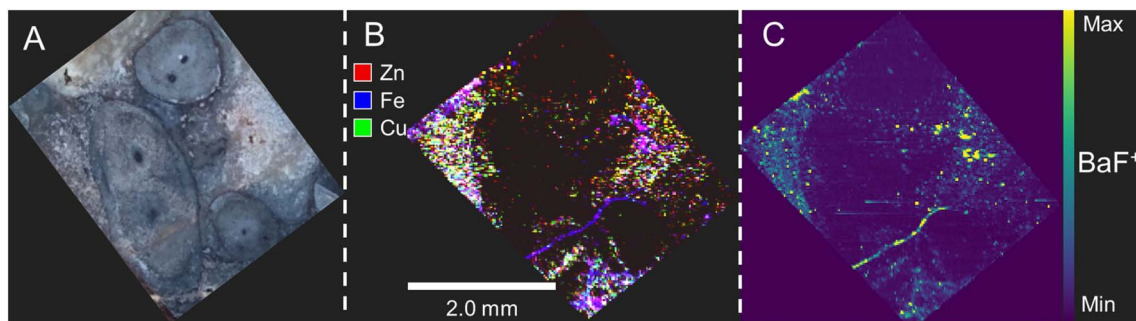
Fig. 6 (A) Photograph of the analysed Rhynie chert. (B) Zn, Fe and Cu were analysed as typical elements found in this mineral. (C) Distribution of F.

in earth science is far from complete[29] and methods capable of investigating the spatial abundance of F in various geologic specimens may improve our understanding of F in the lithosphere. Additionally, it is desirable to trace F in rocks, as it can be used to detect the presence of other elements which occur with it (such as rare earths and lithium) and which are needed in large amounts for future technology.

In this proof of concept, the chert was selected because it is known to be mineralized by F^-. It consists of plant fossils, about 410 million years old, preserved by the activity of a hot spring. The spring waters deposited silica which entered the cells of the plants. However like modern hot springs, the water contained volatile elements and anions including fluorine,[11] which precipitated the mineral fluorite (CaF_2) and which were probably incorporated into clay minerals deposited between the plant fossils. The sample was selected to include both silicified plant fossils and intervening clay minerals. Fig. 6A shows a photograph of the Rhynie chert. The distribution of abundant clay minerals (Zn, Fe, Cu) is shown in B and the distribution of F is shown in C. Both, clay minerals and F were found to be colocalised and to be distributed heterogeneously throughout the sample. The silicified plant fossils (the larger rounded objects in Fig. 6A) showed no significant F abundance. However, the clay (the white chalky matter in the upper left and centre right of Fig. 6A) contained elevated levels of F. This was expected, as clay minerals such as Zn, Fe and Cu maps are known to absorb and incorporate F as a substituting anion. The level of substitution may be very low, but it is effectively detected by this technique.

Conclusions

A novel LA-ICP-MS method for the spatially resolved mapping of F was developed and applied in a proof of concept. A Ba^{2+} solution was used as a modifier and introduced *via* liquid nebulisation into the plasma. F originating from the dry laser aerosol was mixed with the modifier to form BaF^+ in the plasma for subsequent MS analysis. For the method development and to estimate figures of merit, gelatine-based F standards were prepared in-house and LODs and LOQs were found to be in the low µg g^{-1} (at 65 µm resolution) or upper ng g^{-1} range (at 150 µm resolution) depending on the spatial resolution. The developed method was employed to map the F distribution in two human tooth samples

as well as in a Rhynie chert as representative biological and geological samples, respectively. It was possible to interrogate the F distribution in these materials and to generate qualitative F maps. This method closes an important analytical gap by enabling the interrogation of F distributions and its colocalization with other (trace) elements. Future studies will require dedicated matrix-matched standard materials to enable quantitative considerations. While this study used empirically adapted parameters to enable a proof of concept, a systematic approach to understand and model Ba^+, Ba^{2+}, F and F^- formation and localisation in the plasma would likely contribute to further improved limits of analysis, which may promote the analysis of trace F amounts as well as improved spatial resolutions.

Conflicts of interest

The authors declare no conflicts of interest.

Acknowledgements

References

1 D. Kanduti, P. Sterbenk and B. Artnik, *Mater. Soc. Med.*, 2016, **28**, 133–137.

2 M. C. M. Wong, J. Clarkson, A.-M. Glenny, E. C. M. Lo, V. C. C. Marinho, B. W. K. Tsang, T. Walsh and H. V. Worthington, *J. Dent. Res.*, 2011, **90**, 573–579.

3 M. Martinez, G. J. Harry, E. N. Haynes, P.-I. D. Lin, E. Oken, M. K. Horton, R. O. Wright, M. Arora and C. Austin, *J. Anal. At. Spectrom.*, 2023, **38**, 303–314.

4 R. Gonzalez de Vega, A. Cameron, D. Clases, T. M. Dodgen, P. A. Doble and D. P. Bishop, *J. Chromatogr. A*, 2021, **1653**, 462423.

5 K. Steenland and A. Winquist, *Environ. Res.*, 2021, **194**, 110690.

6 N. L. A. Jamari, J. F. Dohmann, A. Raab, E. M. Krupp and J. Feldmann, *J. Anal. At. Spectrom.*, 2017, **32**, 942–950.

7 N. L. A. Jamari, J. F. Dohmann, A. Raab, E. M. Krupp and J. Feldmann, *Anal. Chim. Acta*, 2019, **1053**, 22–31.

1666 | *J. Anal. At. Spectrom.*, 2023, **38**, 1661–1667

This journal is © The Royal Society of Chemistry 2023

8 F. Gelman, M. Muszyńska, J. Karasiński, O. Lev and L. Halicz, *J. Anal. At. Spectrom.*, 2022, **37**, 2282–2285.

9 P. A. Doble, R. Gonzalez de Vega, D. P. Bishop, D. J. Hare and D. Clases, *Chem. Rev.*, 2021, **121**, 11769–11822.

10 S. Rades, E. Ortel, T. Wirth, M. Holzweber, F. Pellegrino, G. Martra and V.-D. Hodoroaba, *Microsc. Microanal.*, 2017, **23**, 1908–1909.

11 C. M. Rice, W. A. Ashcroft, D. J. Batten, A. J. Boyce, J. B. D. Caulfield, A. E. Fallick, M. J. Hole, E. Jones, M. J. Pearson, G. Rogers, J. M. Saxton, F. M. Stuart, N. H. Trewin and G. Turner, *J. Geol. Soc.*, 1995, **152**, 229–250.

12 M. T. Westerhausen, T. E. Lockwood, R. Gonzalez de Vega, A. Röhnelt, D. P. Bishop, N. Cole, P. A. Doble and D. Clases, *Analyst*, 2019, **144**, 6881–6888.

13 L. Schultes, R. Vestergren, K. Volkova, E. Westberg, T. Jacobson and J. P. Benskin, *Environ. Sci.: Processes Impacts*, 2018, **20**, 1680–1690.

14 T. E. Lockwood, M. T. Westerhausen and P. A. Doble, *Anal. Chem.*, 2021, **93**, 10418–10423.

15 N. L. A. Jamari, A. Behrens, A. Raab, E. M. Krupp and J. Feldmann, *J. Anal. At. Spectrom.*, 2018, **33**, 1304–1309.

16 H. Lindner and A. Bogaerts, *Spectrochim. Acta, Part B*, 2011, **66**, 421–431.

17 S. Meyer, R. Gonzalez de Vega, X. Xu, Z. Du, P. A. Doble and D. Clases, *Anal. Chem.*, 2020, **92**, 15007–15016.

18 D. Clases, R. Gonzalez de Vega, S. Funke, T. E. Lockwood, M. Westerhausen, R. V. Taudte, P. A. Adlard and P. Doble, *J. Anal. At. Spectrom.*, 2020, **35**, 728–735.

19 M. Horstmann, R. Gonzalez de Vega, D. P. Bishop, U. Karst, P. Doble and D. Clases, *J. Anal. At. Spectrom.*, 2021, **36**, 767–775.

20 D. Clases, M. Ueland, R. Gonzalez de Vega, P. Doble and D. Pröfrock, *Talanta*, 2021, **221**, 121424.

21 D. P. Bishop, D. Clases, F. Fryer, E. Williams, S. Wilkins, D. J. Hare, N. Cole, U. Karst and P. A. Doble, *J. Anal. At. Spectrom.*, 2016, **31**, 197–202.

22 R. Gonzalez de Vega, T. E. Lockwood, X. Xu, C. Gonzalez de Vega, J. Scholz, M. Horstmann, P. A. Doble and D. Clases, *Anal. Bioanal. Chem.*, 2022, **414**, 5671–5681.

23 H. Kabir, A. K. Gupta and S. Tripathy, *Crit. Rev. Environ. Sci. Technol.*, 2020, **50**, 1116–1193.

24 WHO, *A Ser. World Heal. Organ. Monogr.*, 2006.

25 M. Mohapatra, S. Anand, B. K. Mishra, D. E. Giles and P. Singh, *J. Environ. Manage.*, 2009, **91**, 67–77.

26 S. J. Kashyap, R. Sankannavar and G. M. Madhu, *J. Hazard. Mater. Lett.*, 2021, **2**, 100033.

27 C. for D. C. and Prevention, *Monit. Fluorid. United States*, cited 2018, Spring 15, https://www.cdc.gov/fluoridation/statistics/index.htm.

28 D. B. Thomas, N. Basu, E. A. Martinez-Mier, B. N. Sánchez, Z. Zhang, Y. Liu, R. P. Parajuli, K. Peterson, A. Mercado-Garcia and M. Bashash, *Environ. Res.*, 2016, **150**, 489–495.

29 K. T. Koga and E. F. Rose-Koga, *C. R. Chim.*, 2018, **21**, 749–756.

This journal is © The Royal Society of Chemistry 2023

J. Anal. At. Spectrom., 2023, **38**, 1661–1667 | **1667**